GUT MICROBIOTA

Neurogenesis and prolongevity signaling in young germ-free mice transplanted with the gut microbiota of old mice

Parag Kundu[1,2,3]*, Hae Ung Lee[1], Isabel Garcia-Perez[4], Emmy Xue Yun Tay[5], Hyejin Kim[1], Llanto Elma Faylon[2], Katherine A. Martin[1], Rikky Purbojati[2], Daniela I. Drautz-Moses[2], Sujoy Ghosh[6,7,8], Jeremy K. Nicholson[9], Stephan Schuster[2], Elaine Holmes[4,10], Sven Pettersson[1,2,11]*

The gut microbiota evolves as the host ages, yet the effects of these microbial changes on host physiology and energy homeostasis are poorly understood. To investigate these potential effects, we transplanted the gut microbiota of old or young mice into young germ-free recipient mice. Both groups showed similar weight gain and skeletal muscle mass, but germ-free mice receiving a gut microbiota transplant from old donor mice unexpectedly showed increased neurogenesis in the hippocampus of the brain and increased intestinal growth. Metagenomic analysis revealed age-sensitive enrichment in butyrate-producing microbes in young germ-free mice transplanted with the gut microbiota of old donor mice. The higher concentration of gut microbiota–derived butyrate in these young transplanted mice was associated with an increase in the pleiotropic and prolongevity hormone fibroblast growth factor 21 (FGF21). An increase in FGF21 correlated with increased AMPK and SIRT-1 activation and reduced mTOR signaling. Young germ-free mice treated with exogenous sodium butyrate recapitulated the prolongevity phenotype observed in young germ-free mice receiving a gut microbiota transplant from old donor mice. These results suggest that gut microbiota transplants from aged hosts conferred beneficial effects in responsive young recipients.

INTRODUCTION

Aging is a biological process associated with gradual impairment in physiological functions. It is likely that the changes associated with aging are recognized by the indigenous gut microbiota that has coevolved together with its host as part of the "holobiont" (*1*, *2*). The composition of the gut microbiota changes with age in both humans and in genetically homogeneous mice raised under controlled experimental conditions (*1*). Recently, a number of studies involving nonmammalian model organisms such as worms, flies, and fish have documented the functional relevance of the gut microbiota in the host aging process (*1*, *3*–*5*). Shifts in the gut microbiota of an aged host are thought to contribute to typical aging phenotypes, including decreased gut epithelial barrier integrity and associated low-grade systemic inflammation (*6*, *7*). However, the unique microbial signatures in centenarians characterized by an enrichment in health-associated microbes (*8*), and the recent findings of adult neurogenesis in the brains of healthy elderly individuals (*9*) underscore the limits of our current understanding of how the gut microbiota changes during aging.

[1]Lee Kong Chian School of Medicine, Nanyang Technological University, Singapore 308232, Singapore. [2]Singapore Centre for Environmental Life Sciences Engineering, Singapore 637551, Singapore. [3]The Center for Microbes, Development and Health, Key Laboratory for Microbiota-Host Interactions, Institut Pasteur of Shanghai, Chinese Academy of Sciences, Shanghai 200031, China. [4]Division of Computational and Systems Medicine, Department of Surgery and Cancer, Sir Alexander Fleming Building, Imperial College London, SW72AZ London, UK. [5]Department of Biological Sciences, Faculty of Science, National University of Singapore, Singapore 117557, Singapore. [6]Duke-NUS Medical School, Singapore 169857, Singapore. [7]National Heart Research Institute, Singapore 169609, Singapore. [8]Pennington Biomedical Research Center, Baton Rouge, LA 70808, USA. [9]Australian National Phenome Center, Murdoch University Perth, Perth, Western Australia, WA6150 Australia. [10]UK Dementia Research Institute at Imperial College London, Burlington Danes Building, Hammersmith Hospital, London, W12 0NN, UK. [11]Department of Neurobiology, Care Sciences and Society, Karolinska Institute, SE 17 177 Stockholm, Sweden.
*Corresponding author. Email: parag.kundu@ips.ac.cn, pkundu@ntu.edu.sg (P.K.); sven.pettersson@ki.se (S.P.)

RESULTS

Age-dependent alterations in the gut microbiota of mice

To assess the influence of the gut microbiota on host aging, we transplanted the gut microbiota from healthy old (~24-month-old) donor mice into young (5- to 6-week-old) germ-free recipient mice (Fig. 1A). Groups of germ-free mice (recipients) were "conventionalized" by both fecal transplantation via gavage and short-term cohousing with respective donors to allow transfer of both the gut and skin microbiota. The ex–germ-free recipient mice were subsequently raised in a contained environment (i.e., in germ-free isolators) and received a defined diet to reduce the influence of confounding factors such as diet or environment. Mouse recipients transplanted with the gut microbiota of age-matched (5- to 6-week-old) young donors served as experimental controls. Metagenomic analysis of stool samples from the young and old donors revealed distinct differences between their gut microbiotas (fig. S1, A and B), in line with previous reports (*6*, *10*). For instance, old donors showed a reduced abundance of bacteria of the *Akkermansia* and *Alistipes* genera in their stool samples (fig. S1B).

Similarities in the gut microbiotas of young donors and their corresponding recipients [young microbiota-transplanted recipient mice (young MT recipients)] and between the old mouse donors and their recipients [old microbiota-transplanted recipient mice (old MT recipients)] confirmed successful gut microbiota transfer (fig. S1C). Metatranscriptomic analysis revealed distinct gene expression patterns for the gut microbiotas of young versus old donors and for young MT recipients versus old MT recipients, suggesting functional divergence in the gut microbiotas of young compared to old mice (fig. S1D). Compared to the gut microbiota transcriptomes of young donors and young MT recipients, those of the old donors and old MT recipients showed elevated expression of fumarate reductase, an enzyme required for anaerobic respiration (fig. S1E).

Colonization of germ-free recipients with the gut microbiota from healthy old donors had no adverse effects on age-associated weight

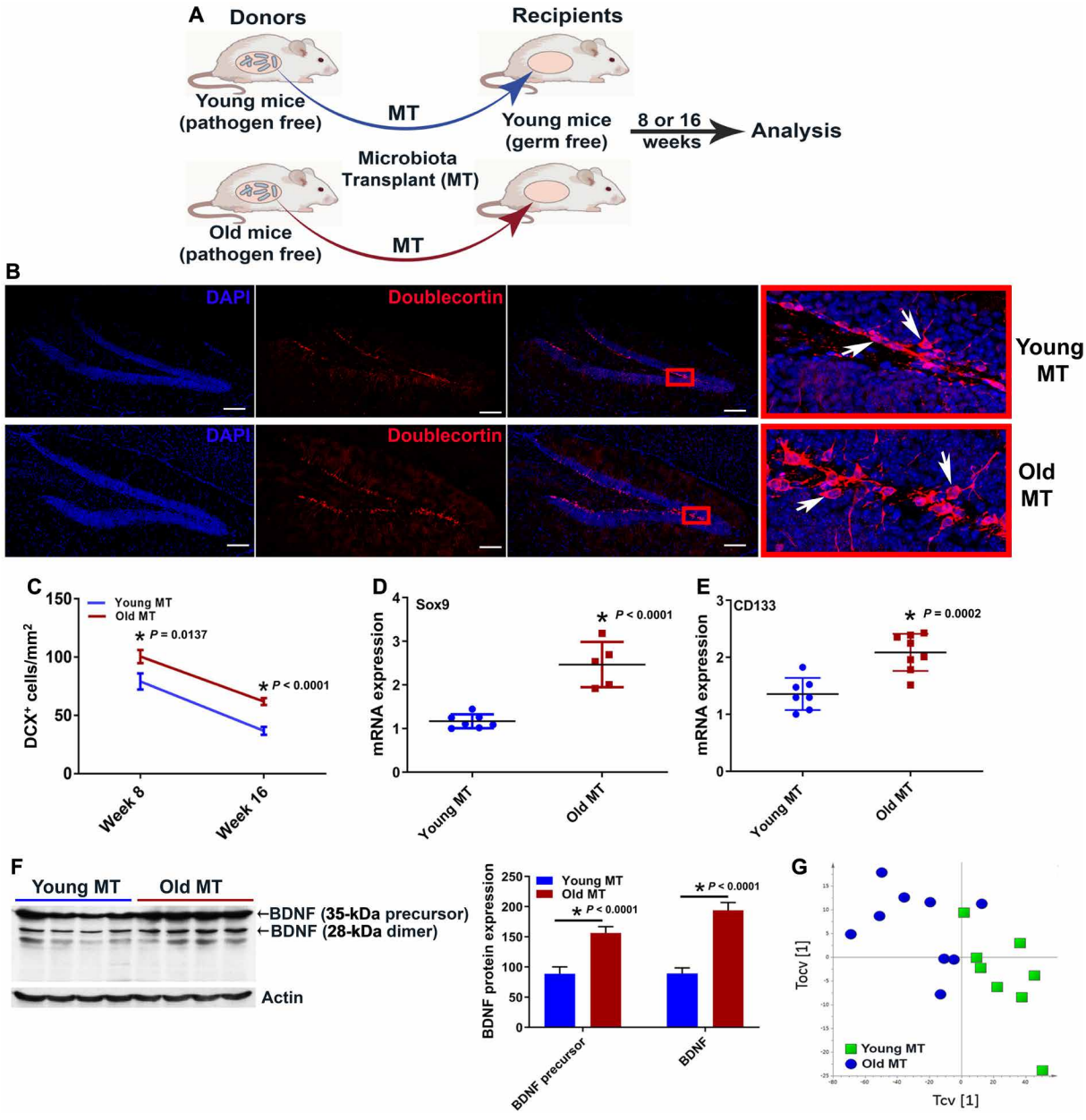

Fig. 1. Gut microbiota transplants from old donor mice promote hippocampal neurogenesis in germ-free recipient mice. (**A**) Gut microbiota transplants (MTs) from ~24-month-old or 5- to 6-week-old mice were transplanted into 5- to 6-week-old germ-free young recipient mice. The transplanted mice were subjected to short-term cohousing with donors and then were housed in a controlled environment for 8 or 16 weeks before being euthanized. (**B**) Shown are representative images of doublecortin (DCX)–stained neurons in the dentate gyrus of young recipient mice receiving a gut microbiota transplant from old or young donors, referred to as old MT recipients or young MT recipients, respectively. DCX staining is red, and DAPI counterstain is blue. The white arrows indicate DCX^+ neurons, and the red boxes indicate the area magnified in the two left panels. Scale bars, 100 μm. (**C**) Shown is quantification of the number of DCX^+ neurons in the dentate gyrus of old MT and young MT recipient mice ($n = 5$ per group). (**D** and **E**) Shown is the expression of Sox9 (D) and CD133 (E) mRNA in the hippocampus of old MT and young MT recipient mice ($n \geq 5$ per group). (**F**) Western blot analysis and quantification of BDNF protein expression in the hippocampus of old MT and young MT recipient mice ($n = 4$ per group). Actin was used as the loading control. (**G**) Differences in hippocampal metabolites between old MT and young MT recipient mice ($n = 8$ per group). The model is composed of one predictive (tcv [1]) and one orthogonal (tocv [1]) principal components. Data are reported as means ± SEM. *P calculated using the Student's t test.

gain (fig. S2A), food intake (fig. S2B), or muscle weight gain (fig. S2C). Likewise, there were no differences in blood glucose (fig. S2D), serum insulin (fig. S2E), triglycerides (fig. S2F), or cholesterol (fig. S2G) in young MT recipients versus old MT recipients. Similarly, multiple behavioral tests showed no notable differences in phenotypes such as anxiety between these two groups (fig. S2, H to J).

Mouse recipients of gut microbiota transplants from old donors show an increase in doublecortin-positive hippocampal neurons

Aging is typically associated with reduced adult neurogenesis in the brain and gradual changes in inflammatory gene expression signatures in various organs including the brain and gut (*1*, *11*). Furthermore,

abnormal changes in gut microbiota composition have been linked to age-associated neurodegenerative diseases, such as Alzheimer's disease and Parkinson's disease (*12*, *13*). This prompted us to investigate adult neurogenesis in the dentate gyrus of the hippocampus of young MT recipients compared to old MT recipients. Unexpectedly, 8 weeks after gut microbial transplantation, old MT recipients had more doublecortin-positive (DCX^+) neurons in the dentate gyrus than did young MT recipients, indicating increased neurogenesis in the brains of old MT recipients ($P = 0.0137$) (Fig. 1, B and C). This increase was even more pronounced 16 weeks after gut microbial transplantation ($P < 0.0001$) (Fig. 1, B and C). There were also significant increases in the expression of markers of cellular stemness, including Sox9 ($P < 0.0001$) and CD133 ($P = 0.0002$) in the hippocampus of the brains of old MT recipients compared to young MT recipients (Fig. 1, D and E). However, the number and soma size of microglia, the key immune cells in the brain, were comparable between the two groups with no obvious difference in microglial morphology (fig. S3, A to C). In addition, the expression of hippocampal pro- and anti-inflammatory cytokines including tumor necrosis factor–α (TNFα), interleukin-6 (IL-6), and IL-10 was similar between the two groups (fig. S3, D to F).

We speculated that changes in brain-derived neurotrophic factor (BDNF), a known neurogenic factor regulated by the gut microbial metabolite butyrate (*14*–*16*), might underlie the increased neurogenesis observed in the dentate gyrus of old MT recipients. As expected, the expression of hippocampal BDNF was significantly higher ($P < 0.0001$) in the old MT recipients compared to young MT recipients (Fig. 1F). However, hippocampal expression of tyrosine receptor kinase B (TrkB), the BDNF receptor, was similar among the two groups (fig. S3G). Further, metabolic profiling of hippocampal tissue (Fig. 1G) revealed increased abundance of metabolites such as taurine, choline, glutamate, and γ-aminobutyric acid (GABA) in old MT recipients compared to young MT recipients (Table 1). These metabolites are known to be associated with neurogenesis and maturation of neurons (*17*–*21*). As expected, the number of DCX^+ neurons in the dentate gyrus was lower in the old donor mice compared to the young donor mice ($P < 0.0001$; fig. S3, H and I), confirming that the old donors did not show aberrant neurogenesis. Furthermore, hippocampal expression of the tight junction markers claudin 1, occludin, and zonula occludens-1 (fig. S3, J to L) indicated that there were no major differences in the integrity of the blood-brain barrier between the young MT recipients and old MT recipients (*22*). Together, these results suggested that the gut microbiota of the old donor mice had the ability to support adult hippocampal neurogenesis when transplanted into young mouse recipients.

Table 1. Altered metabolites in the hippocampus of old MT recipient mice measured using ^{1}H NMR. The table lists metabolites, significant chemical shift values and multiplicity, and direction of associated changes. ADP, adenosine diphosphate. Multiplicity key: s, singlet; d, doublet; t, triplet; q, quartet; dd, doublet of doublets; m, multiplet.

Metabolite	Multiplicity	Association
Taurine	3.43 (t), 3.26 (t)	↑
GABA	2.29 (t), 3.02 (t), 1.91 (q) 2.34 (d)	↑
Lactate	1.33 (d), 4.11(q)	↑
Alanine	1.48 (d)	↑
Glutamate	2.05 (m), 2.36 (dd), 3.77 (t)	↑
N-acetyl aspartate	2.02 (s), 2.70 (dd), 2.51 (dd)	↑
Glycerophosphocholine	3.78 (m), 3.67 (dd), 4.36 (m), 3.23 (s)	↑
Phosphocholine	3.22 (s)	↑
Myoinositol	4.06 (t), 3.63 (t), 3.53 (dd)	↑
Creatinine	3.04 (s), 3.93 (s)	↑
ADP	8.58 (s), 8.27 (s)	↑
Choline	3.20 (s)	↑
Unknown 1	7.68 (s)	↓

Gut microbiota transplants from old donors increase intestinal surface area in recipient mice

The increase in adult hippocampal neurogenesis in the old MT recipients prompted us to investigate the intestinal tracts of these animals, given that the intestinal epithelium undergoes rapid cellular turnover under steady-state conditions. Investigation of intestinal morphology revealed increases in the length and width of the villi in the old MT recipients ($P < 0.0001$; Fig. 2, A to C). In addition, both the small intestine and colon were longer in old MT recipients compared to young MT recipients ($P = 0.0001$; Fig. 2, D and E, and fig. S4, A and B). Thus, because of the increase in intestinal length and villi length and width, the intestinal surface area was likely to be increased in the old MT recipients compared to young MT recipients. Moreover, the old MT recipients had deeper intestinal crypts and showed a marked increase in 5-ethynyl-2′-deoxyuridine (EdU)–positive proliferating intestinal crypt cells than did young MT recipients ($P < 0.0001$; Fig. 2, F to H). There were also more mucus-producing goblet cells in the intestines of old MT recipients compared to young MT recipients ($P < 0.0001$; fig. S4, C and D).

A recent study reported low-grade inflammation and a compromised intestinal barrier in germ-free mice transplanted with a dysbiotic gut microbiota from old donor mice (*6*). However, under our experimental conditions, we did not observe a difference in intestinal permeability between the two groups as indicated by the comparable serum concentrations of fluorescein isothiocyanate (FITC) dextran (Fig. 2I). Moreover, the expression of intestinal tight junction proteins, which regulate intestinal barrier integrity (Fig. 2, J to L), and of pro- and anti-inflammatory cytokines (Fig. 2, M to Q) was similar between the young MT recipients and old MT recipients. These findings were further supported by comparable amounts of circulating serum TNFα in young versus old MT recipients (fig. S4E). Microarray analysis of gene expression in the ileum revealed that peroxisome proliferator–activated receptor (PPAR) signaling was the most enriched pathway in the old MT recipients (Fig. 2R, and fig. S4, F and G). This finding is consistent with our other results, as PPAR signaling is critical for intestinal barrier maintenance and epithelial homeostasis and restitution (*23*–*25*).

To investigate the increase in intestinal surface area in the old MT recipients, we examined the donors and found that old donor mice had considerably longer intestines and differences in intestinal morphology compared to the young donor mice (fig. S4, H to L).

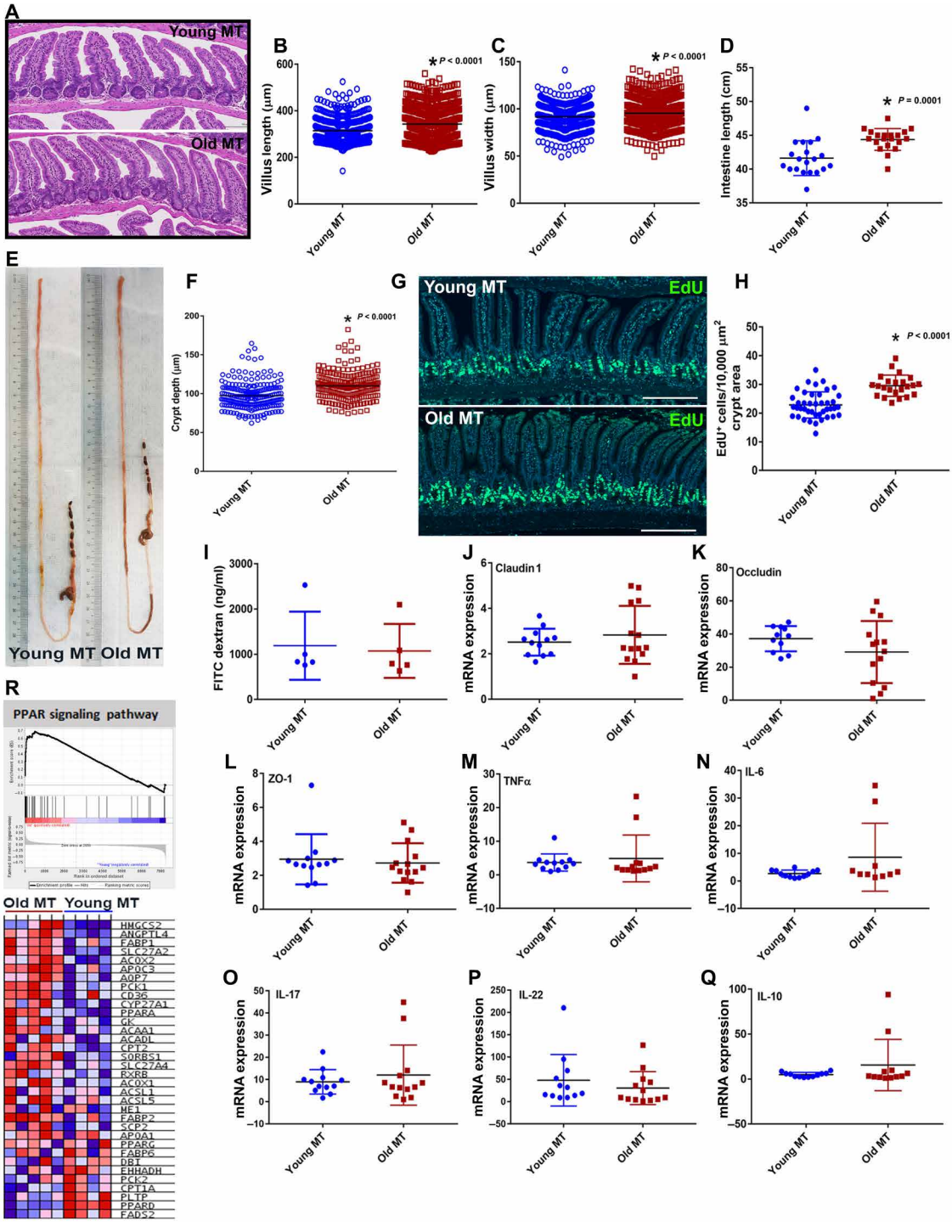

Fig. 2. Gut microbiota transplants from old donor mice promote intestinal growth and surface area expansion. (**A**) Representative images of hematoxylin and eosin staining of the small intestine of old MT and young MT recipient mice. Scale bar, 100 μm. (**B** and **C**) Quantification of villus length (B) and villus width (C) in the jejunum of old MT and young MT recipient mice ($n = 11$ per group). (**D**) Quantification of the length of the intestine from old MT and young MT recipient mice ($n = 20$ per group). (**E**) Representative images showing the intestinal length of old MT and young MT recipient mice. (**F**) Quantification of jejunal crypt depth in old MT and young MT recipient mice ($n = 10$ per group). (**G**) Representative images of jejunum tissue sections from old MT or young MT recipient mice, stained with 5-ethynyl-2′-deoxyuridine (EdU) (green) and DAPI counterstain (blue). Scale bars, 200 μm. (**H**) Quantification of EdU-positive cells in jejunum tissue sections from old MT and young MT recipient mice ($n = 10$ per group). (**I**) Shown is the intestinal permeability of old MT and young MT recipient mice measured by the amount of FITC-dextran in blood after oral gavage ($n = 5$ per group). (**J** to **Q**) Shown is the expression of mRNAs encoding claudin 1 (J), occludin (K), zonula occludens-1 [ZO-1; (L)], TNFα (M), IL-6 (N), IL-17 (O), IL-22 (P), and IL-10 (Q) in the ileum of old MT and young MT recipient mice ($n \geq 10$ per group in each case). (**R**) Heatmap showing enrichment scores for the PPAR signaling pathway (KEGG pathway) in the ileum of old MT and young MT recipient mice. Genes with absolute fold changes of >1.5-fold and false discovery rates (FDR) of <0.05 were considered to be differentially expressed. Data are reported as means ± SEM. *P calculated using the Student's t test; *$P < 0.05$ is considered significant.

Our finding that old donor mice had longer intestines is in line with previous reports (*26*), although the molecular mechanisms underlying this phenotype are not completely known. A reasonable explanation could be the decline in *Akkermansia muciniphila* in the gut microbiota of the old hosts (fig. S1B) as this bacterial strain is known to regulate host intestinal length and surface area (*27*).

Germ-free mice transplanted with old donor gut microbiota show metabolic changes in the liver and increased butyrate production

Next, we focused on the liver to better understand the impact of transplanting the gut microbiota of old donors on the metabolism of germ-free recipients. Old MT and young MT recipients displayed

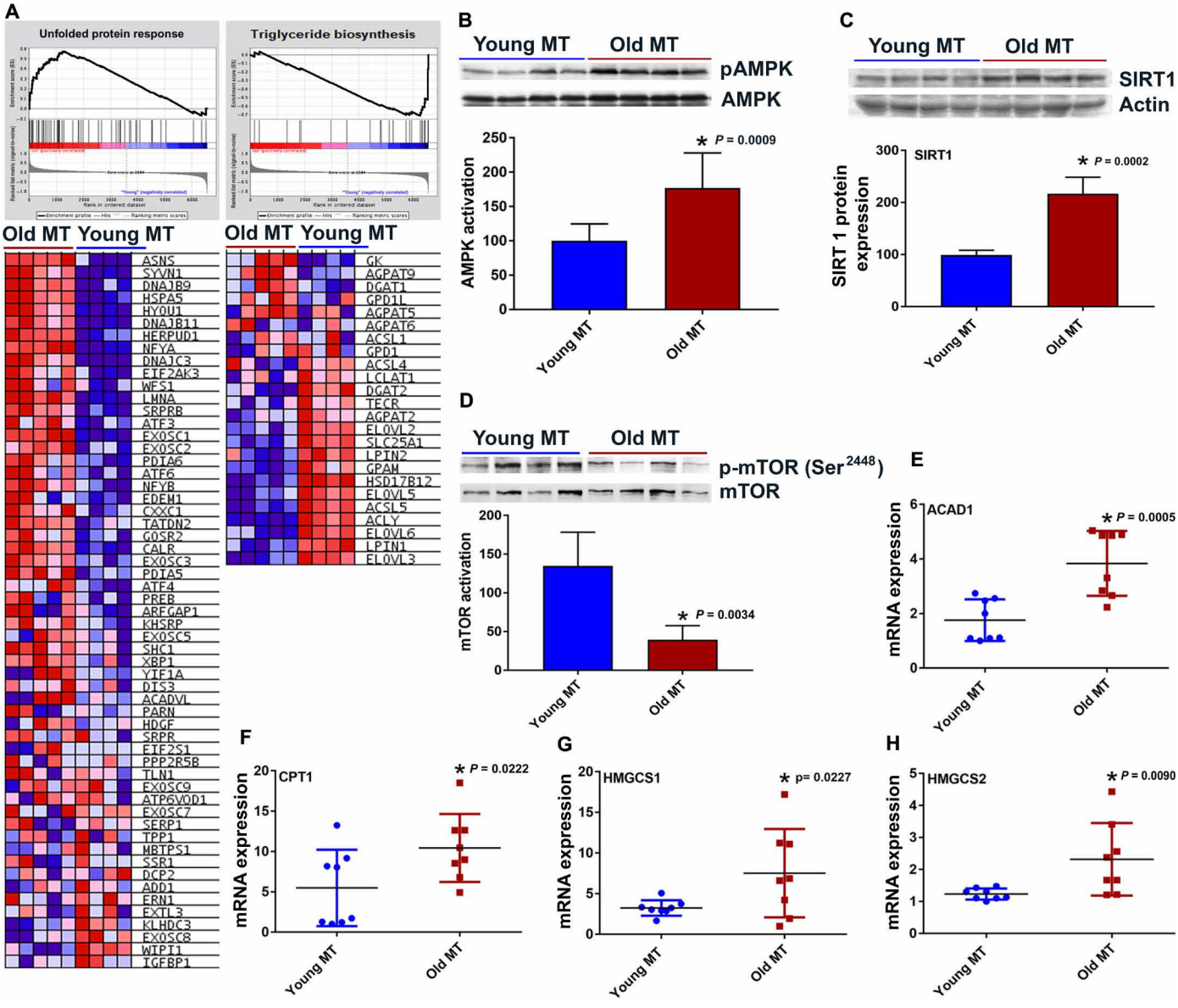

Fig. 3. Recipient mice transplanted with old donor gut microbiota show distinct metabolic signatures. (**A**) Heatmap shows enrichment scores for the unfolded protein response (UPR) and triglyceride biosynthesis pathways in the liver of old MT and young MT recipient mice. Genes with absolute fold changes of >1.5-fold and FDR of <0.05 were considered to be differentially expressed. (**B**) Western blotting and quantification of AMPK activation in the liver of old MT and young MT recipient mice ($n = 8$ per group). Phosphorylated AMPK (pAMPK), a measure of AMPK activation, was normalized to total AMPK. (**C**) Western blotting and quantification of SIRT1 protein in the liver of old MT and young MT recipient mice ($n = 4$ per group). Actin was used as the loading control. (**D**) Western blotting and quantification of mTOR activation in the liver of old MT and young MT recipient mice ($n = 4$ per group). Phosphorylated mTOR (p-mTOR), a measure of mTOR activation, was normalized to total mTOR. (**E** to **H**) Shown is the expression of mRNAs encoding ACAD1 (E), CPT1 (F), HMGCS1 (G), and HMGCS2 (H) in the liver of old MT and young MT recipient mice ($n = 8$ per group in each case). Data are reported as means ± SEM. *P calculated using the Student's t test.

distinct metabolic signatures in the liver (fig. S5A and table S1). In particular, glutathione, which helps to combat oxidative stress (*28*), was elevated in old MT recipients (table S1) despite similar systemic superoxide dismutase activity between the old MT and young MT recipient groups (fig. S5B). Gene expression array analysis revealed further differences in molecular pathways in the liver between the two groups (fig. S5C). The old MT recipients displayed an increased cytoprotective unfolded protein response (UPR) and a concurrent decline in triglyceride biosynthesis (Fig. 3A). Aging is generally associated with a decline in the stress recognition system and in UPR signaling efficiency, whereas increased stress resistance is a hallmark of longevity (*29*, *30*). Thus, these data suggested a possible microbial link to adaptive stress tolerance in the host, as there was no difference in hepatocyte apoptosis between the old MT and young MT recipients (fig. S5D).

These findings suggested changes in hepatic energy homeostasis. Activation and expression of key energy sensing proteins such as AMP (adenosine 5′-monophosphate)–activated protein kinase (AMPK)

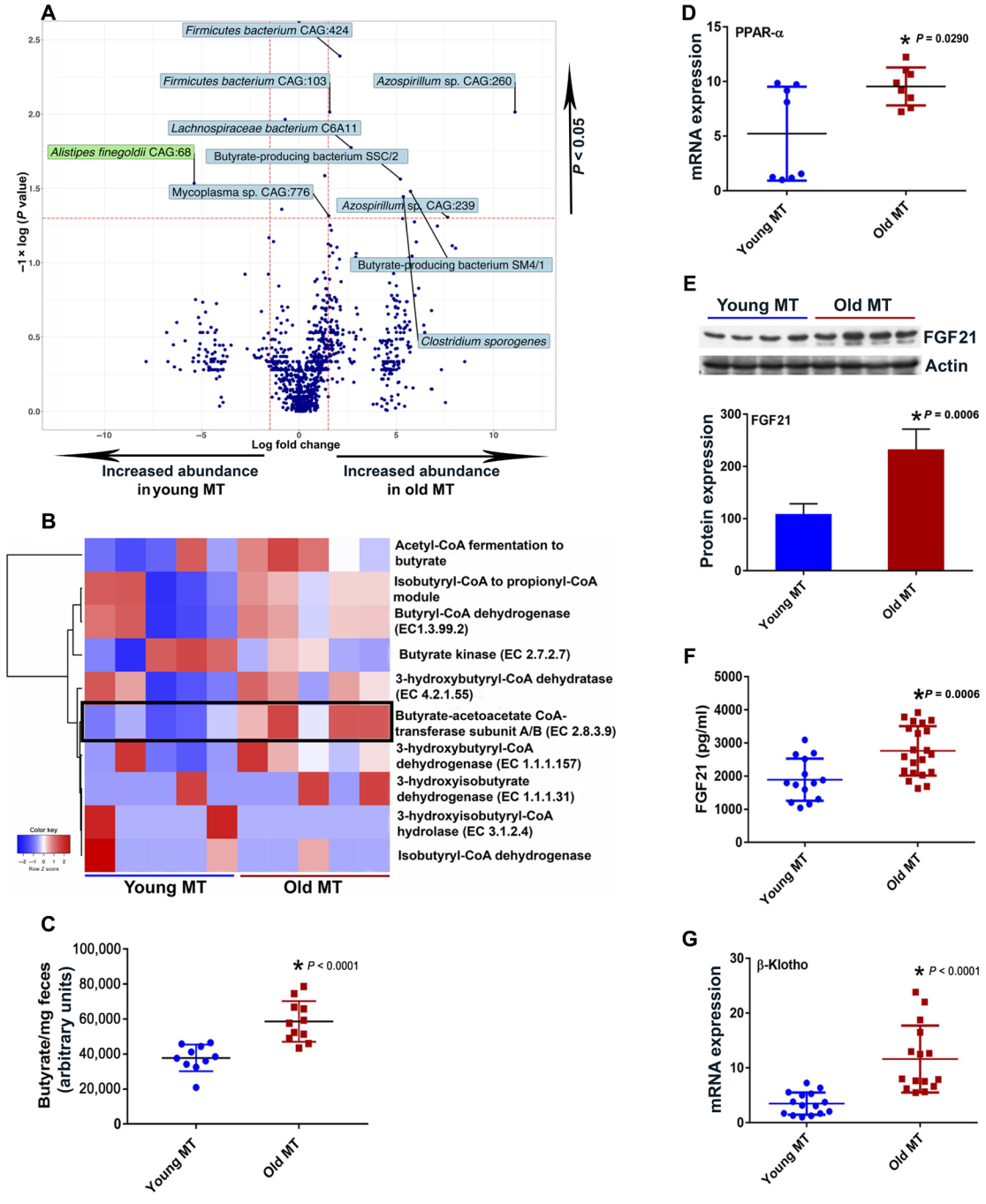

Fig. 4. Recipient mice transplanted with old donor gut microbiota show an increase in butyrate-producing bacteria and FGF21. (**A**) Shown is a metagenomic analysis of the gut microbiota of recipient mice receiving either an old donor gut microbiota transplant (old MT) or a young donor gut microbiota transplant (young MT). The labeled data points show microbial species with a twofold or more difference in abundance and $P < 0.05$. Blue boxes represent enrichment of bacterial species in the gut microbiota of mice receiving old donor transplants, and the green box represents enrichment of bacterial species in the gut microbiota of mice receiving transplants from young donors. (**B**) Shown is a heatmap of the metagenomic analysis showing enrichment of genes involved in the butyrate production pathway according to the SEED subsystem database ($n = 5$ per group). (**C**) Shown is the quantification of butyrate in the feces of young MT and old MT recipients measured using NMR spectroscopy ($n \geq 10$ per group). (**D**) Shown is expression of PPAR-α mRNA in the liver of young and old MT recipient mice ($n = 8$ per group). (**E**) Shown is Western blot analysis and quantification of the FGF21 protein in the liver of young and old MT recipient mice ($n = 4$ per group). Actin was used as the loading control. (**F**) Enzyme-linked immunosorbent assay (ELISA) assay of serum samples showing the amount of circulating FGF21 in young and old MT recipient mice ($n \geq 14$ per group). (**G**) Shown is the expression of mRNA encoding the FGF21 co-receptor β-klotho in the hippocampus of young and old MT recipient mice ($n = 15$ per group). Data are reported as means ± SEM. *P calculated using the Student's t test.

and sirtuin 1 (SIRT1) were elevated in the liver of old MT compared to young MT recipient mice ($P < 0.005$; Fig. 3, B and C, and fig. S5E). In addition, mammalian target of rapamycin (mTOR) activation in the liver was reduced ($P < 0.005$; Fig. 3D), whereas hepatic expression of enzymes regulating β-oxidation and ketogenesis including acyl-coenzyme A dehydrogenase 1 (ACAD1), carnitine palmitoyltransferase 1 (CPT1), 3-hydroxy-3-methylglutaryl-CoA synthase (HMGCS1), and HMGCS2 was increased in the old MT recipient mice ($P < 0.05$; Fig. 3, E to H). However, serum concentrations of leucine and methionine were similar between the two groups (fig. S5, F and G). Collectively, these data suggested that the gut microbiota of an aging host had the ability to trigger prolongevity signaling pathways including those of AMPK, SIRT1, and mTOR when transplanted into a young recipient.

In an attempt to further understand the mechanisms underlying the differences between young MT and old MT recipient mice, we compared their metagenomes. We found an enrichment of butyrate-producing bacteria including Firmicutes and Lachnospiraceae in

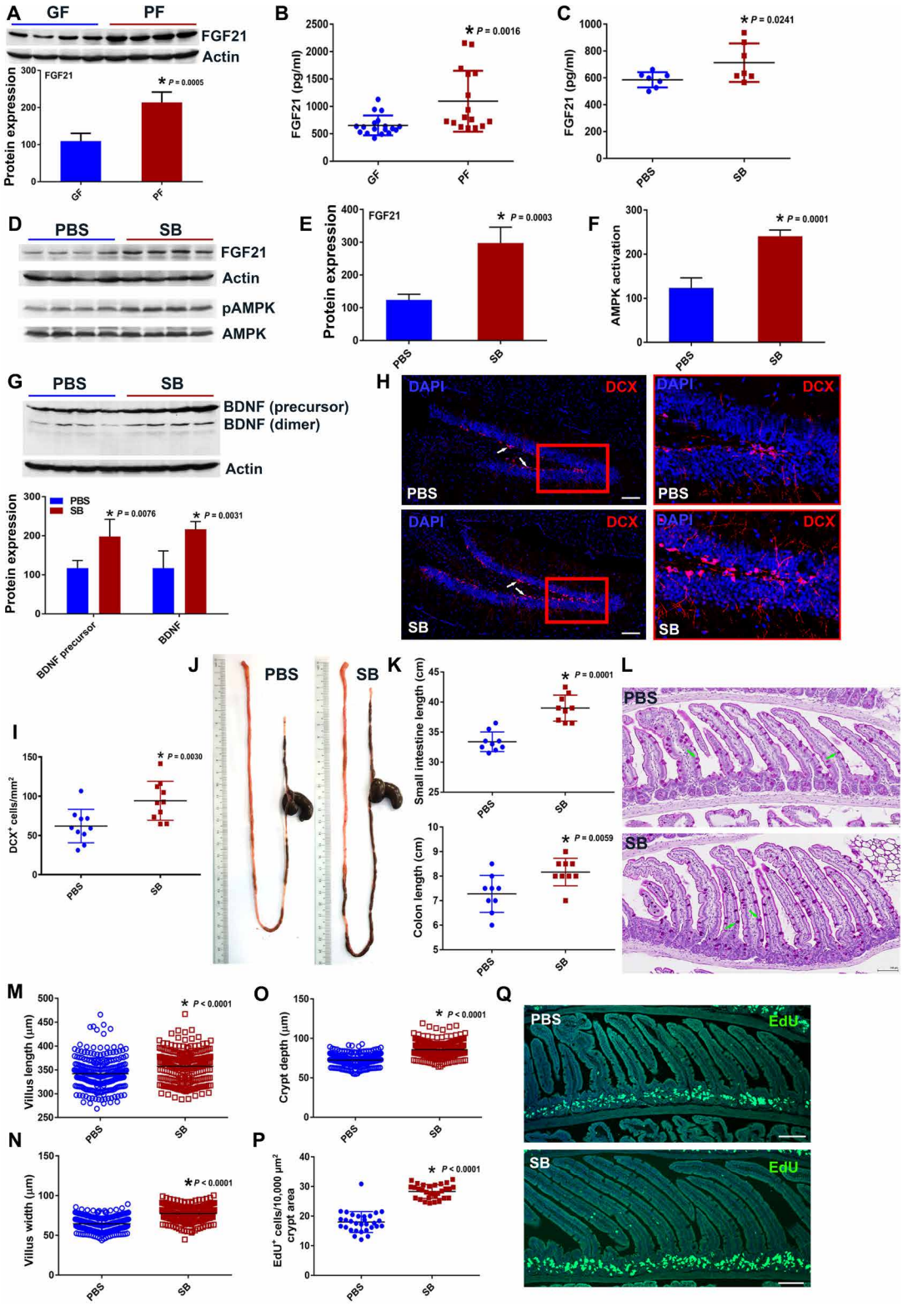

Fig. 5. Treating germ-free mice with sodium butyrate resulted in an old MT recipient phenotype. (**A**) Shown is Western blot analysis and quantification of the FGF21 protein in the liver of young germ-free (GF) mice and conventionally housed [pathogen-free (PF) mice; $n = 4$ per group]. Actin was used as the loading control. (**B**) ELISA assay of serum samples showing abundance of circulating FGF21 in germ-free and pathogen-free mice ($n \geq 15$ per group). (**C**) Germ-free C57BL/6 mice aged 5 to 6 weeks were orally administered either sodium butyrate (SB) dissolved in PBS or PBS vehicle alone as control daily for 8 weeks. Shown is an ELISA of serum samples measuring circulating FGF21 in sodium butyrate–treated and vehicle-treated mice ($n = 7$ per group). (**D** to **F**) Shown is Western blot analysis (D) and quantification of hepatic FGF21 (E) protein and AMPK activation (F) in sodium butyrate–treated and vehicle-treated (PBS) germ-free mice ($n = 4$ per group). (**G**) Shown is Western blot analysis and quantification of BDNF protein expression in the hippocampus of sodium butyrate–treated and vehicle-treated (PBS) germ-free mice ($n = 4$ per group). Actin was used as the loading control. (**H**) Representative images showing DCX staining of neurons (red) in the dentate gyrus of sodium butyrate–treated and vehicle-treated germ-free mice (DAPI counterstain, blue). Scale bars, 100 μm. (**I**) Shown is quantification of DCX^+ neurons in the dentate gyrus of sodium butyrate–treated and vehicle-treated germ-free mice ($n = 9$ per group). (**J**) Representative images showing the length of the intestine of sodium butyrate–treated and vehicle-treated germ-free mice. (**K**) Shown is quantification of the lengths of the small intestine and colon of sodium butyrate–treated and vehicle-treated germ-free mice ($n = 9$ per group). (**L**) Representative images of periodic acid–Schiff staining of the jejunum of sodium butyrate–treated and vehicle-treated germ-free mice. Scale bars, 100 μm. (**M** and **N**) Shown is quantification of villus length (M) and villus width (N) in the jejunum of sodium butyrate–treated and vehicle-treated (PBS) germ-free mice ($n = 11$ per group). (**O**) Shown is quantification of jejunal crypt depth of sodium butyrate–treated and vehicle-treated (PBS) germ-free mice ($n = 5$ per group). (**P**) Shown is quantification of cells staining positive for EdU in the jejunum of sodium butyrate–treated and vehicle-treated (PBS) germ-free mice ($n = 9$ per group). (**Q**) Representative images showing EdU staining (green) with DAPI counterstain (blue) of small intestine tissue sections from sodium butyrate–treated and vehicle-treated germ-free mice ($n = 9$ per group). Scale bars, 100 μm. Data are reported as means ± SEM. *P calculated using the Student's t test.

the metagenomes of old MT compared to young MT recipient mice (Fig. 4A). Moreover, butyrate acetoacetate-CoA-transferase, one of the enzymes involved in the terminal step of butyrate synthesis (*31*, *32*), was particularly enriched in the gut microbiota of old MT recipients (Fig. 4B). Nuclear magnetic resonance (NMR) spectroscopy profiling further revealed a significant increase ($P < 0.0001$) in fecal butyrate in the old MT compared to young MT recipients (Fig. 4C). Apart from being the main nutrient source for colonocytes and enhancing gut epithelial barrier integrity (*33*), butyrate also regulates hippocampal BDNF expression (*14*, *15*), potentially linking this microbial signature to the increased neurogenesis observed in old MT recipients.

Germ-free mice transplanted with old donor gut microbiota show FGF21 activation

Butyrate is known to stimulate the expression of the pleiotropic hormone fibroblast growth factor 21 (FGF21) by inhibiting histone deacetylase 3 and consequently activating the transcription factor PPAR-α (*34*). The expression of PPAR-α was found to be increased in old MT compared to young MT recipients ($P < 0.01$; Fig. 4D). In addition, both hepatic expression of FGF21 and its systemic abundance were increased in old MT compared to young MT recipient mice ($P < 0.001$; Fig. 4, E and F). These data may explain, in part, the molecular changes observed in the liver of old MT recipients as FGF21 activates AMPK (*35*), represses lipogenesis and triglyceride accumulation in hepatocytes (*35*, *36*), and is elevated upon UPR activation (*37*). Moreover, hippocampal expression of the FGF21 co-receptor, β-klotho, was also higher in old MT recipient mice ($P < 0.0001$; Fig. 4G). The systemic abundance of FGF21 (fig. S6A), activation of hepatic AMPK (fig. S6, B and C), number of hippocampal DCX^+ neurons (fig. S6, D and E), and intestinal morphology (fig. S6, F to K) were comparable between the young MT recipients (experimental controls) and conventionally raised age-matched mice containing a normal gut microbiota.

The abundance of butyrate-producing microbes in MT recipient mice depends on recipient age

To test the hypothesis that enrichment of butyrate-producing microbes in MT recipient mice was dependent on recipient age and intestinal environment, we transplanted the gut microbiota from young (5- to 6-week-old) or old (~24-month-old) donor mice into old (~18-month-old) germ-free recipient mice (fig. S7A). Gut microbiota transplantation did not have any adverse effects on the body weight of the old recipient mice (fig. S7B). Metagenomic analysis did not show any enrichment of butyrate-producing gut bacteria in the ~18-month-old recipient mice transplanted with either a young or old donor gut microbiota (fig. S7, C and D). Consequently, fecal butyrate and circulating FGF21 were comparable between the ~18-month-old recipient mice transplanted with either an old or young donor gut microbiota (fig. S7, E and F). In addition, the expression of markers for hippocampal neurogenesis and cellular stemness was similar between these two groups of aged recipients (fig. S7, G to J). Similarly, intestinal morphology, gut cell proliferation, and inflammatory status, as well as hepatic metabolism, were also comparable between the two aged recipient groups (fig. S7, K to Y).

Germ-free mice treated with sodium butyrate show the same phenotype as old MT recipient mice

The beneficial effects of an old donor gut microbiota transplant observed in young germ-free recipient mice underscored the need to directly test a potential beneficial role of butyrate. We first confirmed that conventionally housed mice containing a normal gut microbiota (pathogen-free experimental controls) exhibited increased hepatic and circulating FGF21 compared to germ-free mice ($P < 0.005$; Fig. 5, A and B). Next, we orally administered sodium butyrate or phosphate-buffered saline (PBS) vehicle control daily for 8 weeks to young (5- to 6-week-old) germ-free mice. Treatment with sodium butyrate increased the abundance of hepatic and circulating FGF21 compared to young germ-free mice treated with vehicle ($P < 0.05$; Fig. 5, C to E). Moreover, activation of AMPK and expression of SIRT1 were elevated in the liver of sodium butyrate–treated compared to vehicle-treated young germ-free mice ($P < 0.05$; Fig. 5, D and F, and fig. S8A). In addition, BDNF expression and the number of DCX^+ neurons were increased in the hippocampus of sodium butyrate–treated compared to vehicle-treated control mice ($P < 0.01$; Fig. 5, G to I). Furthermore, sodium butyrate–treated mice displayed increased gut epithelial cell proliferation compared to vehicle-treated control mice (Fig. 5, J to Q, and fig. S8B).

DISCUSSION

Here, we attempted to uncover the functional characteristics of the gut microbiota of an aging host using young germ-free mouse recipients transplanted with old or young mouse donor gut microbiota. We showed that cells in the intestine and brain responded to old donor gut microbiota–derived cues. For instance, transplantation of old donor gut microbiota into young germ-free recipient mice enhanced neurogenesis in the hippocampus of the brain and promoted intestinal growth. Furthermore, old donor gut microbiota influenced liver bioenergetics and induced FGF21 expression and catabolic processes such as β-oxidation and ketogenesis in the young mouse recipients. Given that FGF21 can cross the blood-brain barrier, influence neuronal viability (*38*), and, together with β-klotho, promote oligodendrocyte proliferation, remyelination, and central nervous system regeneration (*39*), our findings provide a microbial link to neuroprotective processes.

We also demonstrated that transplantation of the gut microbiota of aged mice increased the abundance of butyrate-producing bacteria and butyrate availability in young recipient mice, thus fostering a butyrate-FGF21–driven metabolic signature. This, in part, may explain the phenotypic differences observed between the old MT and young MT recipients in our experimental setting (fig. S9). Although the phenotypic changes observed in the brain, liver, and intestine of old MT recipients seemed to be microbiota driven, the underlying mechanisms could be a consequence of specific donor microbial signatures or microbial adaptation to a new host environment or a combination of the two. In contrast, old germ-free recipient mice transplanted with gut microbiota from old donor mice failed to respond to the microbial cues under steady-state conditions, thus limiting the beneficial effects observed to the young mouse recipients. This finding underscores our limited understanding of the biology of aging and the intricate interplay between the host and the microbiota during aging. Our data suggest that the gut microbiota's composition and dynamics in a recipient after microbiota transplant is age sensitive and that the early life response to microbial cues may differ considerably from that later in life, consistent with previous studies related to host immune responses (*40*).

Oral administration of sodium butyrate to young germ-free recipient mice induced similar increases in neurogenesis, intestinal

growth, and metabolic (FGF21-AMPK-SIRT1) signatures, as observed in young germ-free mice receiving a gut microbiota transplant from old donors. These findings establish a key role for butyrate in these microbiota-driven phenotypes and are consistent with reports showing butyrate-induced neurogenesis in hippocampus (*41*) and epithelial growth and cellular proliferation in normal intestinal tissue under steady-state conditions (*42*, *43*).

Our study provides new insights into the functional characteristics of the gut microbiota of aging mice. Given the ability of the gut microbiota to respond to dietary, metabolic, and environmental changes, our results imply that the gut microbiota of an old host with metabolic homeostasis may support host health. In contrast, in response to type 2 diabetes or obesity or gut dysbiosis, the gut microbiota could activate inflammatory pathways (*6*). Given that exercise has beneficial effects on BDNF expression and neurogenesis (*44*) and also modulates the gut microbiota (*45*), it is tempting to speculate that exercise may stimulate the enrichment of butyrate-producing bacteria in the gut, but this needs to be investigated in future experiments.

There are several limitations to our study including the lack of longitudinal analysis after gut microbiota transplantation. Given that the dynamics of the gut microbiota change over time even under controlled experimental settings (*1*), such longitudinal approaches are challenging. It is likely that the gut microbiota composition of the transplanted mouse recipients changes as they age during the course of long-term experiments, which could affect experimental outcomes. Another shortcoming of this study involves the inherent limitations of gut microbiota transplantation into germ-free animals, as the experimental outcomes could be affected by the source and quality of microbial inoculum used to reconstitute the gut microbiota in the germ-free recipient mice. It is possible that other microbial metabolites and cellular pathways were also involved in the phenotypic changes observed in the old MT recipients, but these were not investigated in this study.

MATERIALS AND METHODS

Study design

The objective of this study was to elucidate the functional characteristics of the gut microbiota of an aging mouse host. Gut microbiota was transplanted from old (24 months) or young (5 to 6 weeks) donor mice to young germ-free recipient mice (5 to 6 weeks). The recipient mice were housed in contained isolators for 8 or 16 weeks to avoid contamination. During this period, the mice were provided with sterile feed and water ad libitum, and their growth characteristics were monitored. These experiments were repeated several times. At the respective end points, the gut, brain, and liver were analyzed using metabolomic, transcriptomic, and functional approaches. Metagenomic and metatranscriptomic were undertaken to correlate microbial community shifts with altered physiology of the transplanted mouse recipients. We also transplanted the gut microbiota of the same young and old donors into old germ-free recipient mice (~18 months old) to test the importance of host age in responding to microbial cues. To understand the molecular mechanisms underlying the observed phenotypic differences, the microbial metabolite butyrate was administered to young germ-free mice daily for 8 weeks.

In this study, we used cohorts of germ-free mice, pathogen-free mice, conventionalized mice (colonized with donor microbiotas), and butyrate-treated germ-free mice, with a minimum of 10 mice in each experimental group. Researchers were blinded to group allocation, and mice were randomized to groups. All protocols involving animals were carried out in accordance with institutional guidelines of Nanyang Technological University and approved by the Regional Animal Research Ethical Board, Institutional Animal Care and Use Committee, Singapore (protocol no. 2013/SHS/785).

Microbiota transplantation

Specific pathogen-free male C57BL/6 mice aged 5 to 6 weeks (young donors) or ~24 months old (old donors) were used as donors for gut microbiota transplantation, whereas germ-free C57BL/6 mice aged 5 to 6 weeks were used as young recipients in this study. Groups of ~18-month-old germ-free C57BL/6 mice were also used as old recipients for microbiota transplants from young and old donors (age-matched with donors used to transplant young germ-free mice in this study). All mice (pathogen-free donors and germ-free recipients) were fed with a 50:50 combination of autoclavable mouse breeder diet 5021 (LabDiet) and laboratory autoclavable rodent diet 5010 (LabDiet). Groups of germ-free recipient mice were conventionalized using fecal transplantation and short-term cohousing with their respective donors to facilitate the transfer of the entire microbiota (i.e., gut and skin) from the donors to the recipient mice. The recipient mice were subsequently housed in separate confined plastic isolators for 8 or 16 weeks. Experiments using young germ-free recipients were repeated at least five times using 10 mice per group per experiment. All donors and recipients received the same chow throughout the entire course of the experiments, thus excluding any dietary influence on the microbiome composition and function. Briefly, fresh fecal pellets from young or old donor mice were dissolved in sterile PBS by homogenization (using sterile plastic pastel and vigorous shaking), and each recipient mouse was immediately fed with 150 μl of the supernatant using a sterile orogastric gavage to transplant the gut microbiota. The conventionalization procedure was repeated on day 3 after initial inoculation as a booster. Fecal pellets were collected intermittently from the respective recipients to validate conventionalization. Germ-free C57BL/6 mice aged 5 to 6 weeks were used in this study. Groups of germ-free mice were orally gavaged with sterile sodium butyrate (500 mg/kg body weight) dissolved in PBS daily for 8 weeks. Mice gavaged daily with equal volumes of only sterile PBS were used as experimental controls. All mice were fed with a 50:50 combination of autoclavable mouse breeder diet 5021 (LabDiet) and laboratory autoclavable rodent diet 5010 (LabDiet). After 8 weeks, mice from both groups were analyzed.

Groups of 10- to 12-week-old C57BL/6 germ-free and conventionally raised pathogen-free mice containing a normal microbiota were used to analyze the availability of systemic and hepatic FGF21. Groups of 13- to 14-week-old C67BL/6 mice that were conventionally raised, pathogen free, and containing a normal microbiota were used for comparative studies.

Metagenomic and metatranscriptomic analyses

Metagenomic and metatranscriptomic analyses were done on fecal samples collected from donors at the time of initial colonization and from recipients at the end of experiment (8 weeks after colonization).

DNA samples: Before library preparation, the quality of the DNA samples was assessed on a Bioanalyzer 2100 using a DNA 12000 Chip (Agilent). Sample quantitation was carried out using the Invitrogen's Picogreen assay. Library preparation was performed according to Illumina's TruSeq Nano DNA sample preparation protocol. The samples were sheared to ~450 base pair (bp) using a

Covaris S220, following the manufacturer's recommendation, and uniquely tagged with one of Illumina's TruSeq LT DNA barcodes to enable library pooling for sequencing. The finished libraries were quantitated using Invitrogen's Picogreen assay, and the average library size was determined on a Bioanalyzer 2100 using a DNA 7500 chip (Agilent). Library concentrations were then normalized to 4 nM and validated by quantitative polymerase chain reaction (qPCR) on a ViiA-7 real-time thermocycler (Applied Biosystems), using qPCR primers recommended in Illumina's qPCR protocol, and Illumina's PhiX control library as standard. The libraries were then pooled at equimolar concentrations and sequenced in one lane on an Illumina HiSeq2500 sequencer in rapid mode at a read length of 250 bp paired-end.

RNA samples: Before library preparation, the quality of the RNA samples was assessed on a Bioanalyzer 2100 using an RNA 6000 Nano Chip (Agilent). Sample quantitation was carried out using Invitrogen's Ribogreen assay.

Library preparation was performed according to Illumina's TruSeq Stranded mRNA protocol with the following modifications: The oligo-dT mRNA purification step was omitted, and instead, 200 ng of total RNA was directly added to the Elution2-Frag-Prime step. The PCR amplification step, which selectively enriches for library fragments that have adapters ligated on both ends, was performed according to the manufacturer's recommendation, but the number of amplification cycles was reduced to 12. Each library was uniquely tagged with one of Illumina's TruSeq LT RNA barcodes to enable library pooling for sequencing.

The finished libraries were quantitated using Invitrogen's Picogreen assay, and the average library size was determined on a Bioanalyzer 2100 using a DNA 7500 chip (Agilent). Library concentrations were then normalized to 4 nM and validated by qPCR on a ViiA-7 real-time thermocycler (Applied Biosystems), using qPCR primers recommended in Illumina's qPCR protocol, and Illumina's PhiX control library as standard. The libraries were then pooled at equimolar concentrations and sequenced in one lane on an Illumina HiSeq2500 sequencer in rapid mode at a read-length of 100 bp paired-end.

The raw metagenomic and metatranscriptomic Illumina reads were quality and adapter trimmed using cutadapt 1.8.1 with parameters of "-q 20 --minimum-length 30".

The trimmed metagenomic reads were then mapped against the mm10 mouse genome with bowtie2 2.2.5 (*46*) using "-D 20 -R 3 -N 1 -L 20 -i S,1,0.50" as its sensitivity parameters. Any reads that cannot be confidently mapped against the mouse genome (with --unconc switch) were separated and processed as the microbiome reads. Afterward, each microbiome paired-end reads were locally assembled between read 1 and its corresponding read 2 using FLASH 1.2.6 (*47*), with minimum overlapping of 10 bp and error ratio of 0.25. These reads were then aligned against National Center for Biotechnology Information (NCBI) nonredundant protein database (downloaded at 8 April 2015) with RAPSearch2 2.15 (*48*). On the basis of these alignments, the microbial taxonomical classification was determined using the lowest common ancestor algorithm implemented in MEGAN5 (*49*) (parameters: maxmatches=25 minscore=100 minsupport=25). The normalized classification table from MEGAN5 was then used for subsequent statistical analysis in R 3.4.0.

The trimmed metatranscriptomic reads were mapped against the mm10 mouse genome with TopHat2 2.0.13 (*50*). Afterward, the unmapped reads were locally assembled using FLASH 1.2.6. The merged reads were then separated into its ribosomal RNA and nonribosomal RNA components using sortMeRNA 2.0 (*51*). Afterward, the ribosomal RNA reads were processed with QIIME 1.8.0, and the nonribosomal RNA reads were processed with RAPSearch2 and MEGAN5 analysis pipeline.

In vivo proliferation assay and immunofluorescence staining

Intestinal tissues from mice were Swiss-rolled, fixed in 4% formaldehyde, and sectioned. To visualize proliferative cells, mice were intraperitoneally injected with 500 μg of EdU in 100 μl of sterile PBS and euthanized 2 hours later (*52*). Intestinal rolls were sectioned and stained for EdU using the Click-iT Alexa Flour 488 Imaging Kit, following the manufacturer's protocol. Images were captured using Nikon ECLIPSE Ti microscope system. EdU-marked cells were counted using Fiji (ImageJ) (*53*). Statistical analysis was performed in GraphPad Prism 5 (GraphPad Software). $P < 0.05$ was considered significant. For DCX staining, the brains were fixed in 4% paraformaldehyde, equilibrated in 20% sucrose, and sectioned in the coronal plane at 16 μm using Cryostat (Leica). DCX was labeled with a rabbit polyclonal antibody (diluted 1:500; Cell Signaling Technology), Iba-1 was labeled with a rabbit polyclonal antibody (diluted 1:500; Wako) and visualized using Alexa Fluor 594–conjugated secondary goat anti-rabbit antibody (diluted 1:500; Sigma-Aldrich), and nuclei were labeled with 4′,6-diamidino-2-phenylindole (DAPI). Hippocampal dentate gyrus imaging was performed using confocal microscope (Leica STED). Whole area of dentate gyrus was visualized by mosaic stitch procedure of Leica LasX. DCX^+ cells were counted in whole dentate gyrus images of hippocampus. The obtained cell numbers were normalized by the size of dentate gyrus (DCX^+ cell number/mm^2).

Metabolic phenotyping analysis

Sample treatment for ^{1}H NMR metabolic phenotyping analysis

Hydrophilic metabolites were extracted from serum, liver, and hippocampal tissues. Samples were homogenized (64,000 rpm, 2 min) in 7.5 ml of chloroform:methanol (2:1). The homogenate was combined with 1 ml of water, mixed by vortexing, and centrifuged at 13,000*g* for 5 min. The upper aqueous phase was separated from the lower organic phase and dried using nitrogen gas. The hydrophilic phase of each sample was reconstituted in 540 μl of D_2O and 60 μl of phosphate buffer [(pH 7.4) 80% D_2O] containing 1 mM internal standard 3-(trimethylsilyl)-[2,2,3,3,-2H4]-propionic acid (TSP).

^{1}H NMR metabolic phenotyping analysis

^{1}H NMR spectroscopy was performed on the aqueous phase extracts at 300 K on a Bruker 600 MHz spectrometer (Bruker Biospin, Karlsruhe, Germany) using the following standard one-dimensional (1D) pulse sequence with saturation of the water resonance (*54*) RD – gz,1 – 90° – t – 90° – tm – gz,2 – 90° – ACQ, where RD is the relaxation delay, 90° represents the applied 90° radio frequency (rf) pulse, t1 is an interpulse delay set to a fixed interval of 4 μs, RD was 2 s, and tm (mixing time) was 100 ms. Water suppression was achieved through irradiation of the water signal during RD and tm. For the hippocampus and liver samples, each spectrum was acquired using 4 dummy scans, followed by 32 scans and collected into 64 K data points. A spectral width of 20,000 Hz was used for all the samples. Before Fourier transformation, the FIDs were multiplied by an exponential function corresponding to a line broadening of 0.3 Hz. ^{1}H NMR spectra were manually corrected for phase and baseline distortions and referenced to the TSP singlet at δ 0.0. Spectra

were digitized using an in-house MATLAB (version R2014a; The MathWorks Inc., Natwick, MA) script. Spectra were subsequently referenced to the internal chemical shift reference (TSP) at δ 0.0. Spectral regions corresponding to the internal standard (δ −0.5 to 0.5) and water (δ 4.5 to 5.5) were excluded. Each spectrum was normalized to the total weight of the sample.

Data treatment and metabolite identifications

Principal components analysis and orthogonal partial least square discriminant analysis were performed with Pareto scaling in SIMCAP+14 Pareto scaling was applied to all data variables. The robustness of the models was evaluated on the basis of R^2 (explained variance) and Q^2 (capability of prediction) values, as well as seven-fold cross-validation and class permutation validation. Confirmation of significant NMR metabolite identities was obtained using 1D and 2D NMR experiments (spike-in of chemical standards, J-resolved spectroscopy, total correlation spectroscopy, and heteronuclear single-quantum coherence spectroscopy).

Assessment of fecal butyrate using ^{1}H NMR spectroscopy

The samples were randomized before analysis. The frozen fecal pellets (−80°C) of each sample were weighted, transferred into a 2-ml lysing tube (Precellys Ltd.), and mixed with 500 μl of water (liquid chromatography–mass spectrometry grade, Thermo Fisher Scientific). The samples were vortexed for 10 min at 4°C and subjected to 4 cycles of homogenization using the tissue lyser (Precellys Evolution homogenizer, Bertin Instrument Ltd.) during 40 s at 6500 rpm with a pause of 30 s between each cycle. The samples were centrifuged for 10 min at 4°C at 8000 rpm, and the supernatants were collected into a separate Eppendorf tube. The remaining pellets were further extracted by adding 500 μl of water and using the same steps as described above. The supernatants obtained from the two runs of extraction were combined and centrifuged for 12 min at 12,000 rpm. A volume of 630 μl of the supernatant was mixed with 70 μl of potassium phosphate buffer (pH 7.4) (*54*) in a new Eppendorf tube. A volume of 600 μl of the sample was transferred into an NMR tube with an outer diameter of 5 mm before NMR analysis.

The fecal water samples were analyzed using a NOESY preset sequence (NOESYPR1D) with water presaturation on a Avance III Bruker NMR spectrometer (Bruker Biospin, Rheinstetten, Germany) operating at 600.13 MHz. All experiments were performed with 32 scans, a 0.01-s mixing time, a delay between the two 90° rf pulses of 4 μs, and a relaxation time of 4 s at a temperature of 300 K. The spectral window was set at 20 parts per million, and 64,000 data points were recorded. A spectrum of 0.2 mM butyrate was also acquired using the same parameters to help butyrate peaks identification. Spectral processing was performed as described previously (*54*). The spectra were referenced to the internal chemical shift reference (TSP) at δ 0.0.

The spectra were digitized using the MATLAB Impact Toolbox developed by the National Phenome Centre (MATLAB version R2017a; The MathWorks Inc., Natwick, MA). The butyrate peak between δ 1.56 and δ 1.57, which did not overlap with other peaks, was integrated using an in-house MATLAB script and normalized to the total weight of the sample.

Statistical analysis

Statistical analysis was performed in GraphPad Prism 5. $P < 0.05$ was considered significant. Data are presented as means ± SEMs unless otherwise stated. Between-group comparisons were carried out using Student's *t* test.

SUPPLEMENTARY MATERIALS

stm.sciencemag.org/cgi/content/full/11/518/eaau4760/DC1

Materials and Methods

Fig. S1. Influence of old donor gut microbiota transplants on young germ-free recipients.

Fig. S2. Systemic effects of old donor gut microbiota transplants on young germ-free recipients.

Fig. S3. Analysis of neuronal markers in gut microbiota–transplanted recipients and their donors.

Fig. S4. Assessment of intestinal morphology in gut microbiota–transplanted recipients and their donors.

Fig. S5. Metabolic effects of old and young donor gut microbiota transplants on germ-free recipients.

Fig. S6. Comparative analysis of young gut microbiota–transplanted recipient mice and conventionally housed mice with a normal gut microbiota.

Fig. S7. Impact of young or old donor gut microbiota transplant on old germ-free recipients.

Fig. S8. Impact of sodium butyrate treatment on germ-free mice.

Fig. S9. Schematic representation of possible pathways involved in the increased hippocampal neurogenesis and prolongevity signatures observed in old MT recipient mice.

Table S1. Altered metabolites in the liver of old MT recipient mice measured using ^{1}H NMR.

Table S2. Details of primers used for RT-PCR analysis of mouse tissues.

Data file S1. Individual-level data for Fig. 1.

Data file S2. Individual-level data for Fig. 2.

Data file S3. Individual-level data for Fig. 3.

Data file S4. Individual-level data for Fig. 4.

Data file S5. Individual-level data for Fig. 5.

View/request a protocol for this paper from *Bio-protocol*.

REFERENCES AND NOTES

1. P. Kundu, E. Blacher, E. Elinav, S. Pettersson, Our gut microbiome: The evolving inner self. *Cell* **171**, 1481–1493 (2017).
2. J. K. Nicholson, E. Holmes, J. Kinross, R. Burcelin, G. Gibson, W. Jia, S. Pettersson, Host-gut microbiota metabolic interactions. *Science* **336**, 1262–1267 (2012).
3. B. Han, P. Sivaramakrishnan, C. J. Lin, I. A. A. Neve, J. He, L. W. R. Tay, J. N. Sowa, A. Sizovs, G. Du, J. Wang, C. Herman, M. C. Wang, Microbial genetic composition tunes host longevity. *Cell* **169**, 1249–1262.e13 (2017).
4. L. Guo, J. Karpac, S. L. Tran, H. Jasper, PGRP-SC2 promotes gut immune homeostasis to limit commensal dysbiosis and extend lifespan. *Cell* **156**, 109–122 (2014).
5. P. Smith, D. Willemsen, M. Popkes, F. Metge, E. Gandiwa, M. Reichard, D. R. Valenzano, Regulation of life span by the gut microbiota in the short-lived African turquoise killifish. *eLife* **6**, e27014 (2017).
6. N. Thevaranjan, A. Puchta, C. Schulz, A. Naidoo, J. C. Szamosi, C. P. Verschoor, D. Loukov, L. P. Schenck, J. Jury, K. P. Foley, J. D. Schertzer, M. J. Larché, D. J. Davidson, E. F. Verdú, M. G. Surette, D. M. E. Bowdish, Age-associated microbial dysbiosis promotes intestinal permeability, systemic inflammation, and macrophage dysfunction. *Cell Host Microbe* **21**, 455–466.e4 (2017).
7. T. Kamo, H. Akazawa, W. Suda, A. Saga-Kamo, Y. Shimizu, H. Yagi, Q. Liu, S. Nomura, A. T. Naito, N. Takeda, M. Harada, H. Toko, H. Kumagai, Y. Ikeda, E. Takimoto, J. I. Suzuki, K. Honda, H. Morita, M. Hattori, I. Komuro, Dysbiosis and compositional alterations with aging in the gut microbiota of patients with heart failure. *PLOS ONE* **12**, e0174099 (2017).
8. E. Biagi, C. Franceschi, S. Rampelli, M. Severgnini, R. Ostan, S. Turroni, C. Consolandi, S. Quercia, M. Scurti, D. Monti, M. Capri, P. Brigidi, M. Candela, Gut microbiota and extreme longevity. *Curr. Biol.* **26**, 1480–1485 (2016).
9. M. Boldrini, C. A. Fulmore, A. N. Tartt, L. R. Simeon, I. Pavlova, V. Poposka, G. B. Rosoklija, A. Stankov, V. Arango, A. J. Dwork, R. Hen, J. J. Mann, Human hippocampal neurogenesis persists throughout aging. *Cell Stem Cell* **22**, 589–599.e5 (2018).
10. M. G. Langille, C. J. Meehan, J. E. Koenig, A. S. Dhanani, R. A. Rose, S. E. Howlett, R. G. Beiko, Microbial shifts in the aging mouse gut. *Microbiome* **2**, 50 (2014).
11. H. G. Kuhn, H. Dickinson-Anson, F. H. Gage, Neurogenesis in the dentate gyrus of the adult rat: Age-related decrease of neuronal progenitor proliferation. *J. Neurosci.* **16**, 2027–2033 (1996).
12. T. Harach, N. Marungruang, N. Duthilleul, V. Cheatham, K. D. Mc Coy, G. Frisoni, J. J. Neher, F. Fåk, M. Jucker, T. Lasser, T. Bolmont, Reduction of Abeta amyloid pathology in APPPS1 transgenic mice in the absence of gut microbiota. *Sci. Rep.* **7**, 41802 (2017).
13. T. R. Sampson, J. W. Debelius, T. Thron, S. Janssen, G. G. Shastri, Z. E. Ilhan, C. Challis, C. E. Schretter, S. Rocha, V. Gradinaru, M. F. Chesselet, A. Keshavarzian, K. M. Shannon, R. Krajmalnik-Brown, P. Wittung-Stafshede, R. Knight, S. K. Mazmanian, Gut microbiota regulate motor deficits and neuroinflammation in a model of Parkinson's disease. *Cell* **167**, 1469–1480.e12 (2016).

14. R. B. Varela, S. S. Valvassori, J. Lopes-Borges, E. Mariot, G. C. Dal-Pont, R. T. Amboni, G. Bianchini, J. Quevedo, Sodium butyrate and mood stabilizers block ouabain-induced hyperlocomotion and increase BDNF, NGF and GDNF levels in brain of Wistar rats. *J. Psychiatr. Res.* **61**, 114–121 (2015).
15. T. Barichello, J. S. Generoso, L. R. Simões, C. J. Faller, R. A. Ceretta, F. Petronilho, J. Lopes-Borges, S. S. Valvassori, J. Quevedo, Sodium butyrate prevents memory impairment by re-establishing BDNF and GDNF expression in experimental pneumococcal meningitis. *Mol. Neurobiol.* **52**, 734–740 (2015).
16. E. J. Huang, L. F. Reichardt, Neurotrophins: Roles in neuronal development and function. *Annu. Rev. Neurosci.* **24**, 677–736 (2001).
17. X. W. Li, H. Y. Gao, J. Liu, The role of taurine in improving neural stem cells proliferation and differentiation. *Nutr. Neurosci.* **20**, 409–415 (2017).
18. G. Quadrato, M. Y. Elnaggar, C. Duman, A. Sabino, K. Forsberg, S. di Giovanni, Modulation of GABAA receptor signaling increases neurogenesis and suppresses anxiety through NFATc4. *J. Neurosci.* **34**, 8630–8645 (2014).
19. S. Ge, D. A. Pradhan, G. L. Ming, H. Song, GABA sets the tempo for activity-dependent adult neurogenesis. *Trends Neurosci.* **30**, 1–8 (2007).
20. M. J. Glenn, E. M. Gibson, E. D. Kirby, T. J. Mellott, J. K. Blusztajn, C. L. Williams, Prenatal choline availability modulates hippocampal neurogenesis and neurogenic responses to enriching experiences in adult female rats. *Eur. J. Neurosci.* **25**, 2473–2482 (2007).
21. L. D. Hachem, A. J. Mothe, C. H. Tator, Glutamate increases in vitro survival and proliferation and attenuates oxidative stress-induced cell death in adult spinal cord-derived neural stem/progenitor cells via non-NMDA ionotropic glutamate receptors. *Stem Cells Dev.* **25**, 1223–1233 (2016).
22. V. Braniste, M. Al-Asmakh, C. Kowal, F. Anuar, A. Abbaspour, M. Toth, A. Korecka, N. Bakocevic, L. G. Ng, P. Kundu, B. Gulyas, C. Halldin, K. Hultenby, H. Nilsson, H. Hebert, B. T. Volpe, B. Diamond, S. Pettersson, The gut microbiota influences blood-brain barrier permeability in mice. *Sci. Transl. Med.* **6**, 263ra158 (2014).
23. E. Mazzon, S. Cuzzocrea, Absence of functional peroxisome proliferator-activated receptor-alpha enhanced ileum permeability during experimental colitis. *Shock* **28**, 192–201 (2007).
24. J. Bassaganya-Riera, K. Reynolds, S. Martino-Catt, Y. Cui, L. Hennighausen, F. Gonzalez, J. Rohrer, A. U. Benninghoff, R. Hontecillas, Activation of PPAR gamma and delta by conjugated linoleic acid mediates protection from experimental inflammatory bowel disease. *Gastroenterology* **127**, 777–791 (2004).
25. P. Kundu, T. W. Ling, A. Korecka, Y. Li, R. D'Arienzo, R. M. Bunte, T. Berger, V. Arulampalam, P. Chambon, T. W. Mak, W. Wahli, S. Pettersson, Absence of intestinal PPARγ aggravates acute infectious colitis in mice through a lipocalin-2-dependent pathway. *PLOS Pathog.* **10**, e1003887 (2014).
26. E. C. Moorefield, S. F. Andres, R. E. Blue, L. Van Landeghem, A. T. Mah, M. A. Santoro, S. Ding, Aging effects on intestinal homeostasis associated with expansion and dysfunction of intestinal epithelial stem cells. *Aging* **9**, 1898–1915 (2017).
27. C. Chevalier, O. Stojanović, D. J. Colin, N. Suarez-Zamorano, V. Tarallo, C. Veyrat-Durebex, D. Rigo, S. Fabbiano, A. Stevanović, S. Hagemann, X. Montet, Y. Seimbille, N. Zamboni, S. Hapfelmeier, M. Trajkovski, Gut microbiota orchestrates energy homeostasis during cold. *Cell* **163**, 1360–1374 (2015).
28. G. Wu, Y. Z. Fang, S. Yang, J. R. Lupton, N. D. Turner, Glutathione metabolism and its implications for health. *J. Nutr.* **134**, 489–492 (2004).
29. A. Salminen, K. Kaarniranta, ER stress and hormetic regulation of the aging process. *Ageing Res. Rev.* **9**, 211–217 (2010).
30. V. M. Labunskyy, M. V. Gerashchenko, J. R. Delaney, A. Kaya, B. K. Kennedy, M. Kaeberlein, V. N. Gladyshev, Lifespan extension conferred by endoplasmic reticulum secretory pathway deficiency requires induction of the unfolded protein response. *PLOS Genet.* **10**, e1004019 (2014).
31. T. P. Bui, J. Ritari, S. Boeren, P. de Waard, C. M. Plugge, W. M. de Vos, Production of butyrate from lysine and the Amadori product fructoselysine by a human gut commensal. *Nat. Commun.* **6**, 10062 (2015).
32. M. Vital, A. C. Howe, J. M. Tiedje, Revealing the bacterial butyrate synthesis pathways by analyzing (meta)genomic data. *MBio* **5**, e00889 (2014).
33. H. M. Hamer, D. Jonkers, K. Venema, S. Vanhoutvin, F. J. Troost, R. J. Brummer, Review article: The role of butyrate on colonic function. *Aliment. Pharmacol. Ther.* **27**, 104–119 (2008).
34. H. Li, Z. Gao, J. Zhang, X. Ye, A. Xu, J. Ye, W. Jia, Sodium butyrate stimulates expression of fibroblast growth factor 21 in liver by inhibition of histone deacetylase 3. *Diabetes* **61**, 797–806 (2012).
35. A. Salminen, A. Kauppinen, K. Kaarniranta, FGF21 activates AMPK signaling: impact on metabolic regulation and the aging process. *J. Mol. Med.* **95**, 123–131 (2017).
36. Y. Zhang, T. Lei, J. F. Huang, S. B. Wang, L. L. Zhou, Z. Q. Yang, X. D. Chen, The link between fibroblast growth factor 21 and sterol regulatory element binding protein 1c during lipogenesis in hepatocytes. *Mol. Cell. Endocrinol.* **342**, 41–47 (2011).
37. S. Jiang, C. Yan, Q. C. Fang, M. L. Shao, Y. L. Zhang, Y. Liu, Y. P. Deng, B. Shan, J. Q. Liu, H. T. Li, L. Yang, J. Zhou, Z. Dai, Y. Liu, W. P. Jia, Fibroblast growth factor 21 is regulated by the IRE1α-XBP1 branch of the unfolded protein response and counteracts endoplasmic reticulum stress-induced hepatic steatosis. *J. Biol. Chem.* **289**, 29751–29765 (2014).
38. J. Mäkelä, T. V. Tselykh, F. Maiorana, O. Eriksson, H. T. Do, G. Mudò, L. T. Korhonen, N. Belluardo, D. Lindholm, Fibroblast growth factor-21 enhances mitochondrial functions and increases the activity of PGC-1α in human dopaminergic neurons via Sirtuin-1. *Springerplus* **3**, 2 (2014).
39. M. Kuroda, R. Muramatsu, N. Maedera, Y. Koyama, M. Hamaguchi, H. Fujimura, M. Yoshida, M. Konishi, N. Itoh, H. Mochizuki, T. Yamashita, Peripherally derived FGF21 promotes remyelination in the central nervous system. *J. Clin. Invest.* **127**, 3496–3509 (2017).
40. T. Olszak, D. An, S. Zeissig, M. P. Vera, J. Richter, A. Franke, J. N. Glickman, R. Siebert, R. M. Baron, D. L. Kasper, R. S. Blumberg, Microbial exposure during early life has persistent effects on natural killer T cell function. *Science* **336**, 489–493 (2012).
41. D. Val-Laillet, S. Guérin, N. Coquery, I. Nogret, M. Formal, V. Romé, L. le Normand, P. Meurice, G. Randuineau, P. Guilloteau, C. H. Malbert, P. Parnet, J. P. Lallès, J. P. Segain, Oral sodium butyrate impacts brain metabolism and hippocampal neurogenesis, with limited effects on gut anatomy and function in pigs. *FASEB J.* **32**, 2160–2171 (2018).
42. S. Plöger, F. Stumpff, G. B. Penner, J. D. Schulzke, G. Gäbel, H. Martens, Z. Shen, D. Günzel, J. R. Aschenbach, Microbial butyrate and its role for barrier function in the gastrointestinal tract. *Ann. N. Y. Acad. Sci.* **1258**, 52–59 (2012).
43. W. Scheppach, Effects of short chain fatty acids on gut morphology and function. *Gut* **35**, S35–S38 (1994).
44. S. H. Choi, E. Bylykbashi, Z. K. Chatila, S. W. Lee, B. Pulli, G. D. Clemenson, E. Kim, A. Rompala, M. K. Oram, C. Asselin, J. Aronson, C. Zhang, S. J. Miller, A. Lesinski, J. W. Chen, D. Y. Kim, H. van Praag, B. M. Spiegelman, F. H. Gage, R. E. Tanzi, Combined adult neurogenesis and BDNF mimic exercise effects on cognition in an Alzheimer's mouse model. *Science* **361**, eaan8821 (2018).
45. A. Dalton, C. Mermier, M. Zuhl, Exercise influence on the microbiome-gut-brain axis. *Gut Microbes* **10**, 555–568 (2019).
46. B. Langmead, S. L. Salzberg, Fast gapped-read alignment with Bowtie 2. *Nat. Methods* **9**, 357–359 (2012).
47. T. Magoc, S. L. Salzberg, FLASH: Fast length adjustment of short reads to improve genome assemblies. *Bioinformatics* **27**, 2957–2963 (2011).
48. Y. Zhao, H. Tang, Y. Ye, RAPSearch2: A fast and memory-efficient protein similarity search tool for next-generation sequencing data. *Bioinformatics* **28**, 125–126 (2012).
49. D. H. Huson, S. Mitra, H. J. Ruscheweyh, N. Weber, S. C. Schuster, Integrative analysis of environmental sequences using MEGAN4. *Genome Res.* **21**, 1552–1560 (2011).
50. C. Trapnell, L. Pachter, S. L. Salzberg, TopHat: Discovering splice junctions with RNA-Seq. *Bioinformatics* **25**, 1105–1111 (2009).
51. E. Kopylova, L. Noe, H. Touzet, SortMeRNA: Fast and accurate filtering of ribosomal RNAs in metatranscriptomic data. *Bioinformatics* **28**, 3211–3217 (2012).
52. P. Kundu, M. Genander, K. Strååt, J. Classon, R. A. Ridgway, E. H. Tan, J. Björk, A. Martling, J. van Es, O. J. Sansom, H. Clevers, S. Pettersson, J. Frisén, An EphB-Abl signaling pathway is associated with intestinal tumor initiation and growth. *Sci. Transl. Med.* **7**, 281ra244 (2015).
53. A. Jurek, M. Genander, P. Kundu, T. Catchpole, X. He, K. Strååt, H. Sabelström, N. J. Xu, S. Pettersson, M. Henkemeyer, J. Frisén, Eph receptor interclass cooperation is required for the regulation of cell proliferation. *Exp. Cell Res.* **348**, 10–22 (2016).
54. A. C. Dona, B. Jiménez, H. Schäfer, E. Humpfer, M. Spraul, M. R. Lewis, J. T. M. Pearce, E. Holmes, J. C. Lindon, J. K. Nicholson, Precision high-throughput proton NMR spectroscopy of human urine, serum, and plasma for large-scale metabolic phenotyping. *Anal. Chem.* **86**, 9887–9894 (2014).

Acknowledgments: We thank T. Wei Ling, A. Amoyo-Brion, J. Selkrig, M. Ang, N. B. Sulaiman, T. K. Huan, A. Kang, and I. Wijerupage Wijesoma for technical help with experiments. **Funding:** This work was supported by the UK Dementia Research Institute (DRI) at Imperial College London. The UK DRI is an initiative funded by the Medical Research Council, Alzheimer's Society, and Alzheimer's Research UK. S.P. is supported by Lee Kong Chian School of Medicine, Singapore; Centre on Environmental Life Sciences Engineering, Nanyang Technological University; Medical and Biological and Environmental Life Sciences (NIMBELS); Nanyang Technological University Food Technology Center (NAFTEC); and TIER 1 grant Ministry of Education and Canadian Institute of Advanced Research (CIFAR). P.K. and S.P. are supported by a Merlion Grant. S.G. is supported by the National Medical Research Council, Ministry of Heath, Singapore. I.G.-P. is supported by a NIHR career development research fellowship (NIHR-CDF-2017-10-032). The views expressed are those of the authors and not necessarily those of the UK National Health Service (NHS), the NIHR, or the UK Department of Health. **Author contributions:** P.K. and S.P. conceived and designed the project. P.K., H.U.L., E.X.Y.T., and L.E.F. performed all animal experiments. P.K. and E.X.Y.T. analyzed all animal data. P.K. and E.X.Y.T. performed histology, Western blotting, reverse transcriptase PCR (RT-PCR), intestinal permeability and proliferation assays, and ELISA experiments and

analyzed data. I.G.-P., J.K.N., and E.H. performed metabolomics experiments and analyzed data. H.U.L. performed immunohistochemistry and analyzed data. H.K. performed RT-PCR experiments. P.K. and K.A.M. performed animal behavioral tests and analyzed data. P.K. and S.G. analyzed microarray data. R.P., D.I.D.-M., and S.S. performed metagenomic and metatranscriptomic experiments and analyzed data. P.K. and S.P. wrote the paper with the assistance of the other authors. **Competing interests:** All authors declare that they have no competing interests. **Data and materials availability:** The Gene Expression Omnibus accession number for the microarray data reported in this paper is GSE130026. The raw sequencing data for the metagenomic and metatranscriptomic experiments have been deposited at NCBI Sequence Read Archive database under the accession identifier SRP192721. For metagenomic and metatranscriptomic experiments involving gut microbiota transplantation in young germ-free recipients, the accession IDs are as follows: metagenomic: SRR8909073-SRR8909081, SRR8909083 and SRR8909026-SRR8909027, and SRR8909032- SRR8909039; metatranscriptomic: SRR8909062-SRR8909072, SRR8909041-SRR8909045, SRR8909047-SRR8909049, and SRR8909082. For metagenomic experiments involving gut microbiota transplantation in old germ-free recipients, the accession IDs are SRR8909050-SRR8909061, SRR8909024-SRR8909025, SRR8909028-SRR8909031, SRR8909040, and SRR8909046.

Submitted 14 June 2018
Resubmitted 11 February 2019
Accepted 20 May 2019
Published 13 November 2019
10.1126/scitranslmed.aau4760

Citation: P. Kundu, H. U. Lee, I. Garcia-Perez, E. X. Y. Tay, H. Kim, L. E. Faylon, K. A. Martin, R. Purbojati, D. I. Drautz-Moses, S. Ghosh, J. K. Nicholson, S. Schuster, E. Holmes, S. Pettersson, Neurogenesis and prolongevity signaling in young germ-free mice transplanted with the gut microbiota of old mice. *Sci. Transl. Med.* **11**, eaau4760 (2019).

Science Translational Medicine

Neurogenesis and prolongevity signaling in young germ-free mice transplanted with the gut microbiota of old mice

Parag Kundu, Hae Ung Lee, Isabel Garcia-Perez, Emmy Xue Yun Tay, Hyejin Kim, Llanto Elma Faylon, Katherine A. Martin, Rikky Purbojati, Daniela I. Drautz-Moses, Sujoy Ghosh, Jeremy K. Nicholson, Stephan Schuster, Elaine Holmes and Sven Pettersson

Sci Transl Med **11**, eaau4760.
DOI: 10.1126/scitranslmed.aau4760

Hidden benefits of a fecal transplant

Our gut microbiota evolves as we age, yet its effects on host physiology are not clearly understood. Kundu *et al.* now attempt to elucidate these effects by transplanting the gut microbiota of either young or old donor mice into young germ-free recipient mice. They report that young germ-free mice receiving gut microbiota transplants from old mouse donors exhibited increased hippocampal neurogenesis, intestinal growth, and activation of the prolongevity FGF21-AMPK-SIRT1 signaling pathways in the liver. Subsequent metagenomic analysis revealed the potential role of butyrate-producing microbes in mediating these effects. These findings collectively suggest that the gut microbiota of an old mouse host may have beneficial effects in a young mouse recipient.

Science Translational Medicine (ISSN 1946-6242) is published by the American Association for the Advancement of Science, 1200 New York Avenue NW, Washington, DC 20005. The title *Science Translational Medicine* is a registered trademark of AAAS.